

Trends and Variability in Stratospheric NO_x Derived From Merged SAGE II and OSIRIS Satellite Observations

Key Points:

- Stratospheric NO₂ from SAGE II and OSIRIS were merged into a single time series from 1984 to 2018 by accounting for daily photochemical variations
- The merged data set showed similar trends and variability to the WACCM chemistry-climate model
- Trends in NO_x reaching 10% per decade were found in the tropical lower stratosphere; the trends are influenced by volcanic aerosol

Correspondence to:

K. Dubé,
kimberlee.dube@usask.ca

Citation:

Dubé, K., Randel, W., Bourassa, A., Zawada, D., McLinden, C., & Degenstein, D. (2020). Trends and variability in stratospheric NO_x derived from merged SAGE II and OSIRIS satellite observations. *Journal of Geophysical Research: Atmospheres*, 125, e2019JD031798. <https://doi.org/10.1029/2019JD031798>

Received 9 OCT 2019

Accepted 16 MAR 2020

Accepted article online 23 MAR 2020

Kimberlee Dubé¹ , William Randel² , Adam Bourassa¹ , Daniel Zawada¹ ,
Chris McLinden³ , and Doug Degenstein¹ 

¹Institute of Space and Atmospheric Studies, University of Saskatchewan, Saskatoon, Saskatchewan, Canada, ²National Center for Atmospheric Research, Boulder, CO, USA, ³Environment and Climate Change Canada, Toronto, Ontario, Canada

Abstract Nitrogen oxides (NO_x) in the stratosphere are produced from N₂O, which is the dominant emission contributing to stratospheric ozone depletion in the 21st century and an important anthropogenic greenhouse gas. Decades worth of observations are required in order to quantify the variability and trends in stratospheric NO_x so that we can better understand their impact on climate. Here we use the Stratospheric Aerosol and Gas Experiment (SAGE) II, a solar occultation instrument that measured NO₂ from 1984 to 2005, and the Optical Spectrograph and InfraRed Imager System (OSIRIS), a limb-scattering instrument that began measuring NO₂ in 2001. By taking advantage of the 4-year overlap between these instruments it was possible to produce a merged data set of stratospheric NO₂, spanning over 34 years. In order to merge the data a photochemical correction was applied to account for the different times of day at which the instruments measure, and to convert the NO₂ to NO_x. A linear regression model was applied to the merged, deseasonalized data set to identify variability associated with long-term trends, the quasi-biennial oscillation (QBO), and volcanic aerosols. High levels of aerosol associated with large volcanic eruptions were found to greatly influence the calculated trend; when volcanic periods are excluded the trend in NO_x is around 10% per decade in the tropical lower stratosphere. In this case, the observed trends and variability from the satellite measurements show overall good agreement with simulations from the whole atmosphere community climate model (WACCM).

1. Introduction

Stratospheric nitrogen species are important components of the Earth's changing climate system and are closely linked with stratospheric ozone. Nitrous oxide (N₂O) is the third most important long-lived greenhouse gas, the first and second most important being carbon dioxide and methane (Prather et al., 2015). The majority of N₂O originates in oceans and soils, but it is also produced by human activities, especially agricultural fertilization (Seinfeld & Pandis, 2006). N₂O is the dominant emission contributing to ozone (O₃) depletion in the stratosphere since the Montreal Protocol resulted in reduced emissions of chlorine and bromine containing halocarbons (Ravishankara et al., 2009). Global N₂O has increased at an average rate of 0.75 ppb per year since the late 1970s (Hartmann et al., 2013), corresponding to an increase of about 2.4% per decade. As N₂O is the main source of stratospheric reactive nitrogen (NO_y), an increase in N₂O is expected to correspond to an increase in NO_y, which is the sum of the nitrogen oxides NO and NO₂ (collectively called NO_x) and reservoir species.

Several earlier studies have calculated trends in NO_x. Randel et al. (1999) determined the linear trend in NO₂ from the Halogen Occultation Experiment (HALOE, Russell et al., 1993) on the Upper Atmosphere Research Satellite (UARS, Barath et al., 1993) from 1993 to 1997. The sunrise and sunset measurements were analyzed separately. Both were found to have significant, positive trends in the tropics from 25 to 35 km. The trends, averaged over 30° S to 30° N, were 3–4% per year around 30 km, with larger values at lower altitudes. In an analysis of NO₂ measurements taken over Lauder, New Zealand, from 1980 to 2000, Liley et al. (2000) found an increasing trend of around 5% per decade in both the sunrise and the sunset measurements. They also noted the large influence of aerosol on NO₂ following the El Chichon and Pinatubo volcanic eruptions in 1982 and 1991, respectively, as well as a minimal solar cycle response. McLinden et al.

(2001) showed that an increasing 3% per decade trend in N_2O was responsible for about 2.4% per decade of the 5% per decade increase in NO_2 found by Liley et al. (2000). Using a chemical transport model, along with the PRATMO photochemical box model (McLinden et al., 2000), they attributed the remainder of the trend in NO_2 to changes in ozone and halogens. More recently, Galytska et al. (2019) used a linear regression model to look at changes in NO_2 measured by the SCanning Imaging Absorption spectroMeter for Atmospheric CHartographY (SCIAMACHY, Bovensmann et al.,) from 2004 to 2012. They observed a significant increase of 15% per decade in the tropical mid-stratosphere. They also saw a hemispheric asymmetry in the change, with a significant decrease of up to 20% per decade in NO_2 in the Southern Hemisphere and a similarly sized significant increase in the Northern Hemisphere.

The variability in NO_x from the Optical Spectrograph and InfraRed Imager System (OSIRIS, Llewellyn et al., 2004) was first studied by Park et al. (2017). They used OSIRIS NO_2 from 2005 to 2014 in conjunction with N_2O , HNO_3 , and O_3 from the microwave limb sounder (Aura/MLS, Waters et al., 2006) to examine variations in NO_y associated with the quasi-biennial oscillation (QBO). The OSIRIS NO_2 was converted to a daily mean NO_x with PRATMO. The measurements were compared with NO_x and O_3 simulations from the Whole Atmosphere Community Climate Model (WACCM), a coupled chemistry-climate model (e.g., Marsh et al., 2013). The QBO is the dominant source of variability in the tropical stratosphere. The OSIRIS NO_x anomalies showed strong QBO variations in the tropics at altitudes above 27 km. The patterns agreed well with NO_x from WACCM and had correlations from 0.65 to 0.85, however the magnitudes of the WACCM anomalies were larger than OSIRIS at pressures lower than 20 hPa (altitudes above about 27 km) by about 20%. The amplitude of the QBO variations was also found to be about 20% larger in WACCM than in MLS N_2O at pressures less than 10 hPa, which suggests that the differences are due to processes in the model rather than a bias in the instruments.

In order to accurately quantify the trend in NO_x it is necessary to have a high quality, long duration data set. Space-based instruments have been measuring nitrogen species in the stratosphere for decades. Two of these are the Stratospheric Aerosol and Gas Experiment II (SAGE II, McCormick 1987) and OSIRIS. SAGE II measured altitude profiles of NO_2 from 1984 to 2005 using solar occultation, while OSIRIS began taking limb-scattered sunlight measurements of NO_2 in 2001 and is still operational today. Together SAGE II and OSIRIS provide over 34 years of NO_2 measurements. Our goal in this work is to take advantage of the 4-year overlap between these instruments to produce a merged, long-term data set of stratospheric NO_2 . Merged data sets from these two instruments have already been produced for ozone and stratospheric aerosol (Bourassa et al., 2014; Rieger et al., 2015), which shows that the sampling during the overlap period is sufficient for merging. A benefit of combining measurements from SAGE II and OSIRIS is that they both measure NO_2 number density on altitude levels, rather than volume mixing ratio on pressure levels, so no external information is required to put them on the same vertical coordinates before merging. The process for merging NO_2 from SAGE II and OSIRIS is developed in this work, and then the merged data set is used to investigate variability and trends in NO_x from 1984 to 2016. NO_x is derived from NO_2 with PRATMO. Monthly mean NO_x from WACCM is also analyzed and compared with the combined SAGE II-OSIRIS NO_x to better understand the results of the trend analysis. NO_x is a critical component of the stratospheric climate system, and this work provides the first long-term observational record to evaluate our understanding and confront models.

2. Data

The OSIRIS instrument has been operating in sun-synchronous orbit on the Odin satellite since October 2001 (Llewellyn et al., 2004; Murtagh et al., 2002). The optical spectrograph scans the limb of the atmosphere to measure vertical profiles of limb-scattered solar irradiance from 280 to 800 nm. There are 15 orbits per day, and each scan takes 90 s, resulting in 100 to 400 profiles each day, depending on the time of year and the scanning range. NO_2 is retrieved from these measurements by spectral fitting in the wavelength range from 435 to 477 nm for altitudes from 10.5 to 39.5 km with a resolution of 2 km (Sioris et al., 2017). Earlier versions of the NO_2 retrieval were developed by Haley et al. (2004) and Bourassa et al. (2011). This analysis uses version 6.0 of the data, from the latest version of the retrieval, described in Sioris et al. (2017). This version of the data includes the drift correction described in Bourassa et al. (2018). With the correction, the drift in OSIRIS O_3 is less than 1% per decade, and we do not expect anything larger in NO_2 . While the drift-corrected

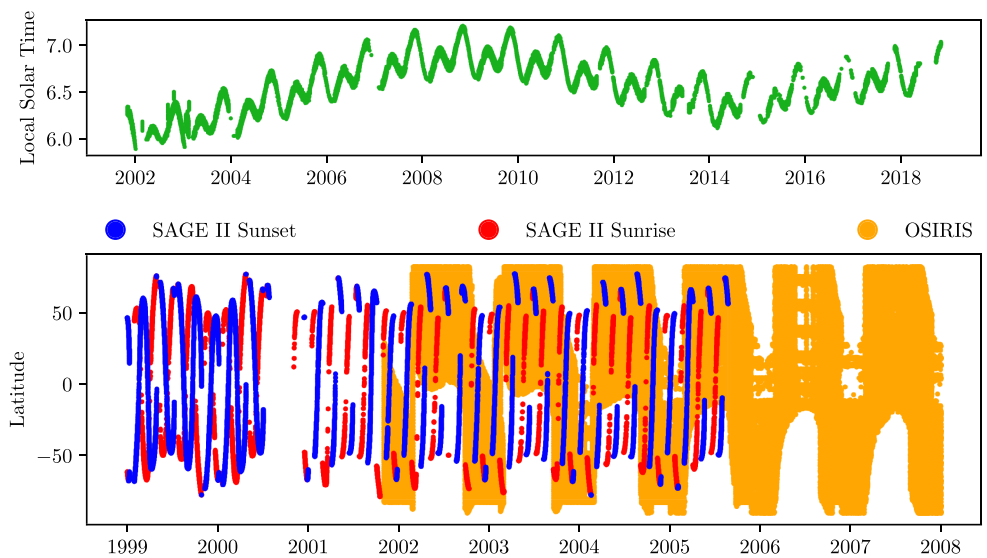


Figure 1. Top: Local solar time of OSIRIS measurements from 5° S to 5° N. Bottom: SAGE II and OSIRIS coverage from 1999 to 2007.

OSIRIS NO₂ has not been validated, the drift in the data was caused by an instrument pointing error and not an issue specific to the ozone retrieval, so any residual effect on NO₂ should be negligibly small. Only the descending node measurements are used. These occur near 6:30 a.m. local solar time, however the exact timing varies by about an hour due to the orbit of the spacecraft. The top panel of Figure 1 shows the time of each measurement from 5° S to 5° N over the course of the mission.

SAGE II scans across the sun to measure the solar irradiance transmitted through the atmosphere at sunrise and sunset. There are 15 sunrise and 15 sunset measurements per day until 2000, after which the number of measurements decreases by half, resulting in only either sunrise or sunset measurements on a given day. During this period the total number of sunrise and sunset measurements overall is quite similar, but more of the sunrise measurements are in the Northern Hemisphere and more of the sunset measurements are in the Southern Hemisphere. The NO₂ retrieval is based on the difference in absorption between Channel 5 (452 nm) and Channel 6 (448 nm) (Damadeo et al., 2013). Data are available from 24 October 1984 to 31 August 2005. Version 7.0 of the data is used in this analysis.

The uncertainties in the SAGE II NO₂ sunset measurements are around 5% in the middle stratosphere and become greater than 10% above 40 km and below 25 km. Our analysis extends to 17.5 km in the extratropics and 20.5 km in the tropics, but we acknowledge the larger uncertainties below 25 km. The sunrise events are considered a “research product.” A thermal shock affects Channels 5 and 6 every time the instrument begins taking measurements, which is challenging to correct for in the case of sunrise events (Damadeo et al., 2013). The sunrise measurements have uncertainties of around 10% in the middle stratosphere, with the uncertainty becoming greater than 50% at altitudes higher than 40 km and lower than 25 km. These uncertainties make it difficult to combine the sunrise measurements with the other data sets. For these reasons it was decided to only use the SAGE II sunset NO₂ in the analysis. A correction to the SAGE II retrieval that accounts for diurnal variations in NO₂ along the line of sight might improve the quality of the retrieved values and is a future area of investigation. This correction is more important for the sunrise measurements than the sunset measurements as the NO_x reactions at sunrise occur more rapidly. A bias in the retrieval could depend on the NO₂ concentrations, but to first order neglecting diurnal variations in the retrieval is unlikely to affect the results presented here as the SAGE II measurements are always at sunset or sunrise, and any remaining bias with OSIRIS that could be caused by the SAGE II retrieval is removed before the data sets are merged. At most we might expect a seasonal effect, which is accounted for in the analysis.

The bottom panel of Figure 1 shows the latitudinal coverage of both SAGE II and OSIRIS from 1999 to 2007. As OSIRIS measures limb-scattered sunlight it cannot take measurements at high latitudes in the winter hemisphere; this results in the gap at winter high latitudes in the bottom panel of Figure 1. The SAGE II measurements with a beta angle (the angle between the orbital plane and the vector to the sun) greater than

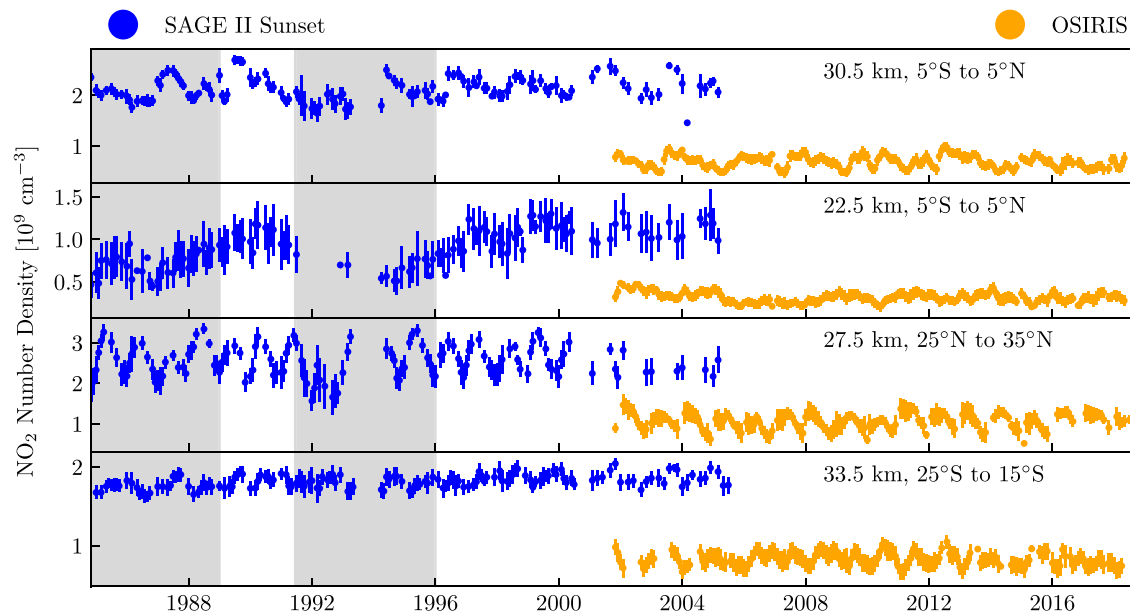


Figure 2. Monthly zonal mean NO_2 number density from SAGE II and OSIRIS in four latitude and altitude bins. The error bars are the standard deviation. The shaded regions denote the time periods influenced by large volcanic eruptions.

$\pm 61^\circ$ are excluded because an assumption about spherical symmetry required by the retrieval is no longer valid at high beta angles (Damadeo et al., 2013).

Figure 2 shows the monthly zonal mean NO_2 number density measured by OSIRIS and SAGE II at sunset, in four latitude and altitude bins. The bins were chosen to represent a range of latitudes and altitudes. The error bars in the figure are the standard deviations of the monthly means. Values with an uncertainty greater than 100% were removed from each instrument data set, as well as any outliers determined as values further than four median absolute deviations from the median. The amount of SAGE II data in the overlap period is sparse at some latitudes, for example, in the third panel of Figure 2. However, the SAGE II ozone and aerosol have the same data sampling and were able to be merged with OSIRIS. The merged SAGE II/OSIRIS ozone data set in particular shows very good agreement with other ozone data sets (e.g., SPARC/IO3C/GAW, 2019), so we do not expect the sparse SAGE II data to cause any inconsistencies.

The shaded regions in Figure 2 denote periods during which the SAGE II NO_2 measurements were affected by large volcanic eruptions. The period from the beginning of the time series to 31 December 1989 corresponds to the El Chichon and Nevado del Ruiz eruptions, while the period from 1 June 1991 to 31 December 1995 corresponds to the Pinatubo volcanic eruption. The analysis is performed both with and without these periods included in order to test the sensitivity of the results to aerosol loading. The QBO variability is clear at 30.5 km in each data set (and at other altitudes/latitudes that are not shown). The main source of bias between the SAGE II sunset and OSIRIS NO_2 is the time of day the measurements were taken within the daily photochemical cycle. The directions of the biases are as expected—the NO_2 concentration is greatest at sunset. If the bias caused by measurement time was not corrected, it could cause an increasing trend in the data due to the drift in the OSIRIS measurement time in the more recent part of the time series.

The instrument results are compared to the output from WACCM, a coupled chemistry-climate model that extends from the surface of the Earth to approximately 140 km (Marsh et al., 2013). The model has 66 vertical levels and a horizontal resolution of 1.9° , latitude by 2.5° , longitude (Marsh et al., 2013). This study uses the average statistical results of five model runs spanning the period from 1955 to 2014 with different initial conditions following the REF-C1 scenario. The REF-C1 scenario includes forcing from observed sea surface temperatures, greenhouse gases, ozone depleting substances, volcanic aerosols, the 11-year solar cycle, and the QBO (Morgenstern et al., 2017; Randel et al., 2017). The equatorial zonal winds associated with the QBO have been nudged to match observations. The five model runs are very similar, with correlations in the monthly means greater than 0.8 at most latitudes and pressure levels.

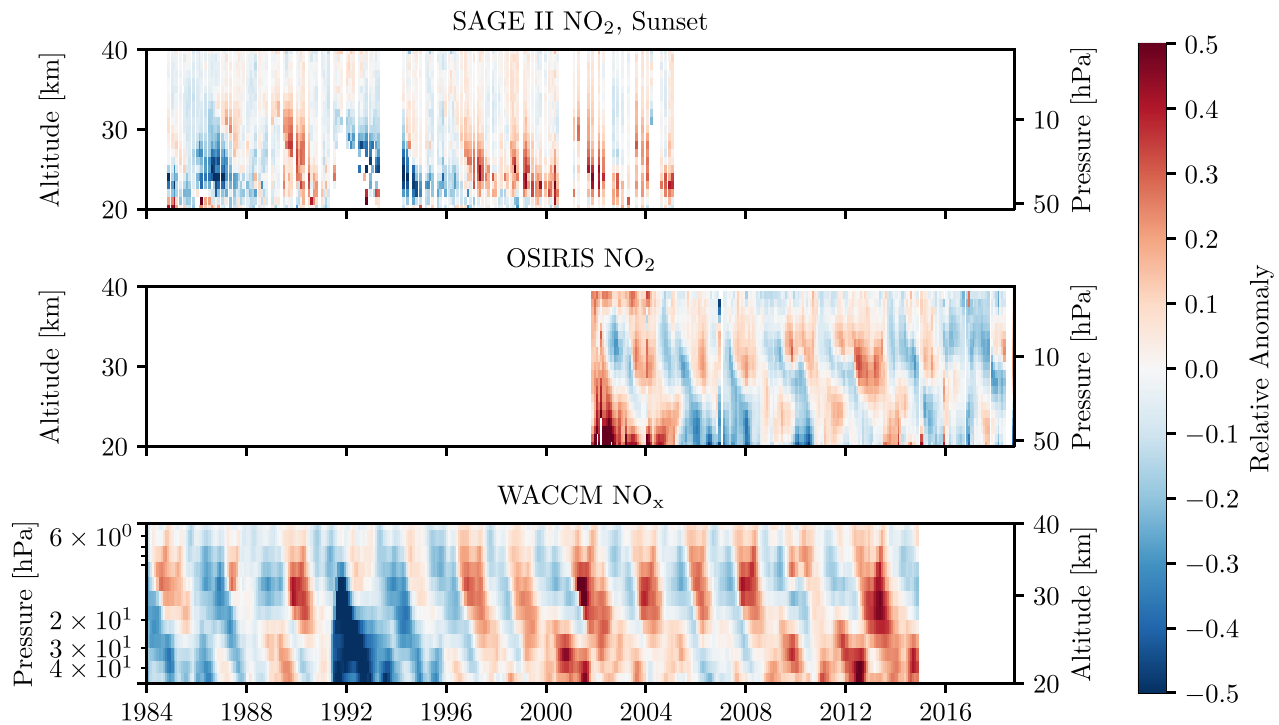


Figure 3. Monthly zonal mean NO_2 relative anomaly in the tropics from SAGE II and OSIRIS and NO_x anomaly from WACCM.

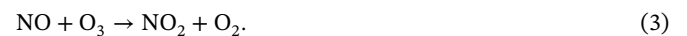
Figure 3 compares the relative anomaly of the monthly mean WACCM NO_x in the tropics from 1984 to 2014 to the relative anomaly in monthly mean NO_2 from SAGE II and OSIRIS. The relative anomaly is unitless and is determined by subtracting the mean of each month from a data set (which removes the seasonal cycle), then dividing by the overall mean. The relative anomaly is used to compare SAGE II and OSIRIS to WACCM because the instrument data are measured as number density and WACCM is computed as volume mixing ratio. There could still be some difference caused by the different units, so this is only done for the purpose of qualitative comparison. The QBO is visible in each data set in Figure 3, however it is less clear in the SAGE II anomalies. Below about 25 km WACCM and OSIRIS become quite different, with OSIRIS having a greater anomaly than WACCM from 2002 to 2005 and WACCM having a greater anomaly from 2008 to 2014. The source of the very high OSIRIS anomaly from 2002 to 2005 is the early local solar time of the measurements relative to the rest of the data (see Figure 1). Above 25 km the magnitude of the WACCM anomaly is greater than the OSIRIS anomaly, which was also observed by Park et al. (2017). The missing SAGE II data at the lower altitudes from 1991 to 1993 are due to an inability to retrieve NO_2 following large aerosol injections from volcanic eruptions. These volcanic periods are still clearly present in WACCM.

3. Photochemical Correction

The nitrogen oxides NO and NO_2 that make up NO_x are interconverted through the reactions



and



During the daytime all three reactions occur rapidly, resulting in an equilibrium between NO and NO_2 . At sunset Reaction 1 ceases production of NO, which results in an increase in NO_2 through Reaction 3. Over the night the concentration of NO_2 decreases as NO_x is converted to other NO_y species. Once the sun rises

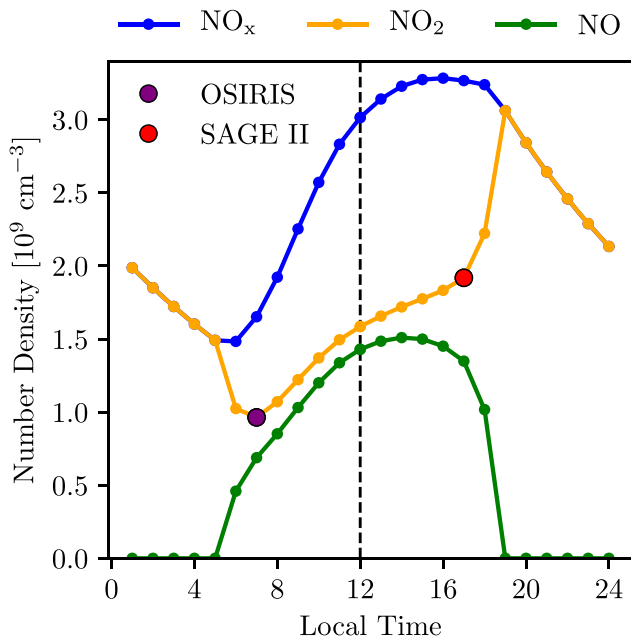


Figure 4. Diurnal cycle in NO_2 , NO , and NO_x at 30.5 km and 3.9° S. Red and purple circles denote the approximate measurement times for SAGE II and OSIRIS.

these are photolyzed back to NO_x , and Reaction 1 begins again, so there is an increase in NO and a decrease in NO_2 (Brasseur & Solomon, 2005).

With OSIRIS and SAGE II sunset we have two sets of measurements taken at different times of day. Figure 4 shows a sample diurnal cycle for each of NO_2 , NO , and NO_x , calculated with the PRATMO photochemical box model. The red dot on the NO_2 line marks the time of the SAGE II measurement, and the purple dot marks the approximate time of the OSIRIS measurement (as mentioned, the exact time varies over the course of the mission). The different local measurement times result in very different NO_2 values due to the daily photochemical cycle. This difference needs to be accounted for before the SAGE II and OSIRIS NO_2 can be combined into a single data set. This is done by shifting all measurements to the same local solar time, using a correction factor determined by PRATMO (McLinden et al., 2000).

PRATMO starts with an input state, then computes a set of chemical reactions over one day and iterates until the start and end values converge (Prather, 1992). The result is a 24 hour steady-state system of all the chemical species included in the model. The inputs required by the photochemical model are ozone, temperature, air density, and pressure profiles. These parameters are kept constant over the course of the day. Both SAGE II and OSIRIS measure ozone profiles coincident with each NO_2 measurement so these are used directly. For SAGE II the pressure and temperature are from the National Centers for Environmental Prediction (NCEP), while for OSIRIS they are from the European Centre for

Medium-Range Weather Forecasts (ECMWF). In both cases they are the values included in the ozone data file and are self-consistent with the retrieval processing. Using different climatologies for each data set is not an issue as the scale factors are calculated for SAGE II and OSIRIS independently. The sensitivity of the PRATMO NO_2 to changes in NO_y , albedo, temperature, O_3 , the NO_2 photolysis rate, and the $\text{NO} + \text{O}_3$ reaction were estimated by perturbing these values in the model. The effect on NO_2 is small. The NO_2 is most sensitive to changes in temperature, where the variation is on the order of -1 degree K per percent change in NO_2 .

PRATMO is used to shift the measurements to a common local solar time of 12:00 pm. Previous studies have used PRATMO to shift the values to 6:30 am, which is the approximate time of the OSIRIS measurements (e.g., Adams et al., 2017; Park et al., 2017). As 6:30 am is very close to the night-day transition region in the photochemical cycle it was found that in some cases shifting the measurements to this time resulted in large and rapidly varying scale factors at high latitudes in winter when 6:30 am was close to sunrise. Adams et al. (2017) avoided this problem for OSIRIS by eliminating measurements close to sunrise: only measurements with a solar zenith angle less than 88°, were used. This is not an option for SAGE II as the solar zenith angle is always 90°. For this work, we shift the measurements to 12:00 pm instead as it is a time of day when the NO_2 curve is smooth.

The outputs of the photochemical model are the number density profiles of various chemical species at specified times of day. The ratio of the NO_2 output from the model at 12:00 pm to the model NO_2 at the initial measurement time (subscript *lst* for local solar time) is used to shift the measured NO_2 to 12:00 pm,

$$[\text{NO}_2]_{12:00}^{\text{meas.}} = [\text{NO}_2]_{lst}^{\text{meas.}} \frac{[\text{NO}_2]_{12:00}^{\text{model}}}{[\text{NO}_2]_{lst}^{\text{model}}} \quad (4)$$

Figure 5 shows the average scale factor from 2002 to 2004 as a function of altitude for each data set in three latitude bins. This is the amount the measured NO_2 is multiplied by to get the NO_2 at noon. A scale factor of less than one means the measurements will be shifted to lower values, and vice versa. The further the scale factor is from one, the further the NO_2 concentration at the measurement time is from the NO_2 concentration at 12:00 p.m. The error bars in Figure 5 are the standard deviation of the average scale factor. The standard deviations of the OSIRIS scale factors are greater because the times of the OSIRIS measurements vary, while SAGE II always measures at sunset.

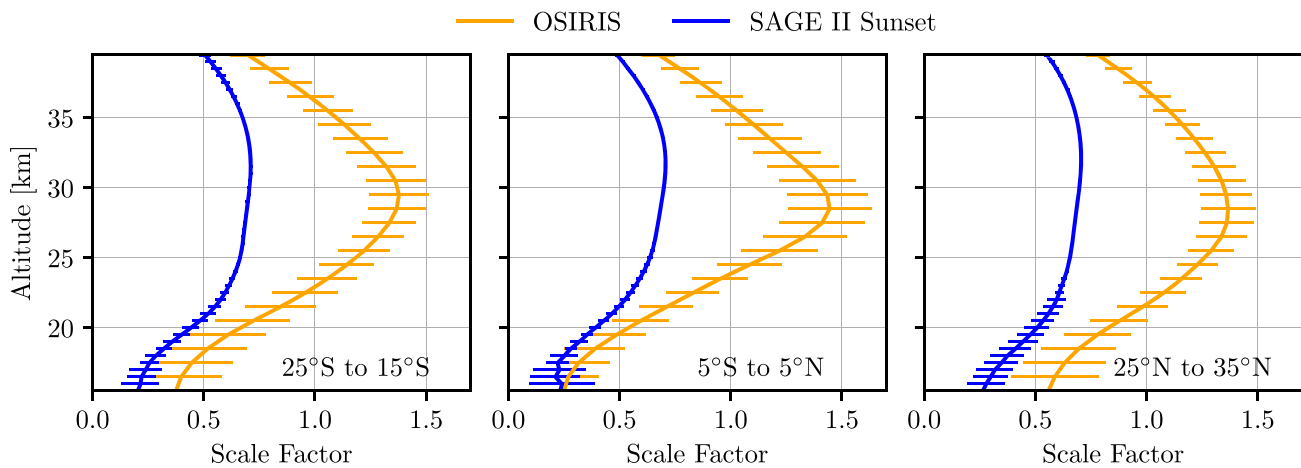


Figure 5. Average scale factor from 2002 to 2004 used to shift the measured NO_2 to 12:00 p.m. as a function of altitude for OSIRIS and SAGE II sunset in three latitude bins. The error bars are the standard deviation.

Figure 6 shows the monthly zonal mean SAGE II and OSIRIS NO_2 after using the photochemical model to shift all the measurements to a common time of 12:00 p.m. There are still biases between the data sets; however, they are smaller than in Figure 2. The SAGE II sunset measurements are biased high compared to OSIRIS. The bias is greatest at lower altitudes and in the tropics.

The right panel of Figure 7 shows the average correlation between the SAGE II sunset and OSIRIS NO_2 time series at 12:00 p.m. for the overlap period from 2002 to 2005. The correlation is greater than 0.6 in much of the stratosphere over 20 to 35 km. The left panel of Figure 7 shows the mean percent difference between SAGE II sunset and OSIRIS NO_2 at 12:00 p.m. Shifting the measurements to a different local solar time with the photochemical model had a minimal effect on the degree of correlation between the two data sets and substantially improved the bias. Although the absolute values are still different, we proceed with merging

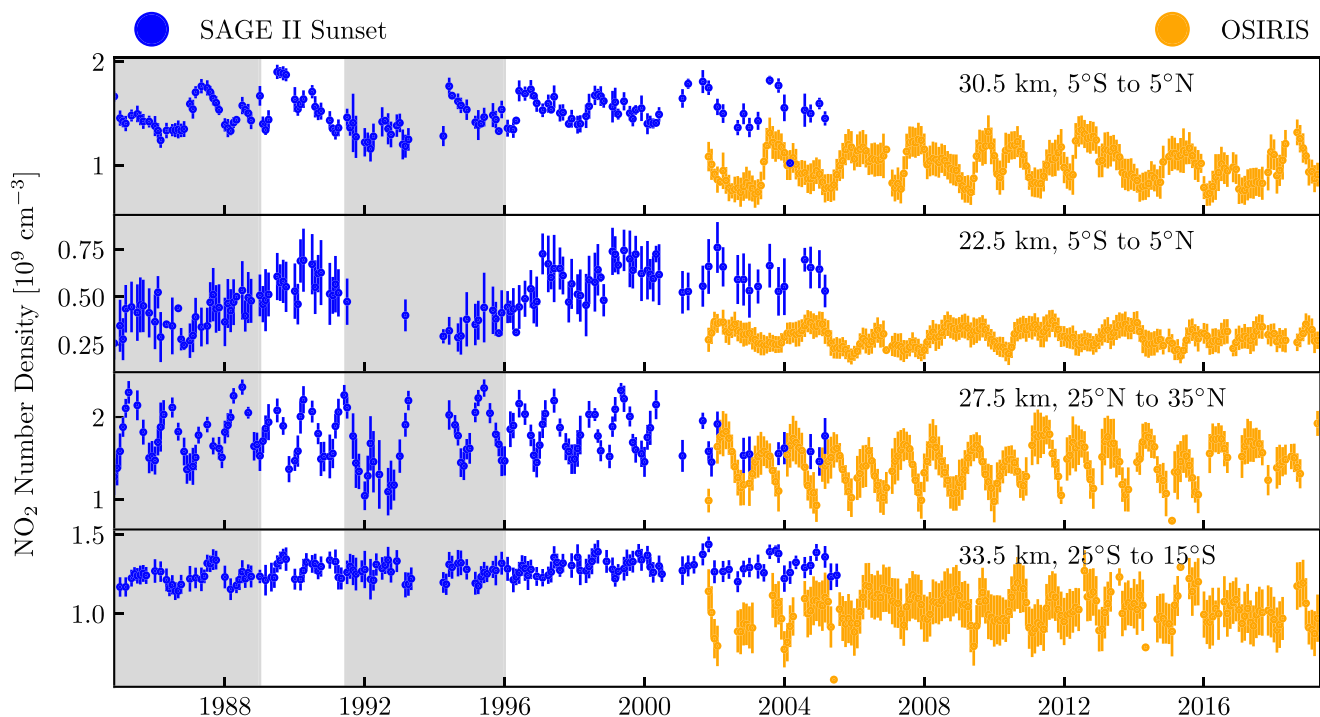


Figure 6. Monthly zonal mean SAGE II and OSIRIS NO_2 as in Figure 2, but with the data shifted to 12:00 local solar time. The shaded regions denote the time periods influenced by large volcanic eruptions.

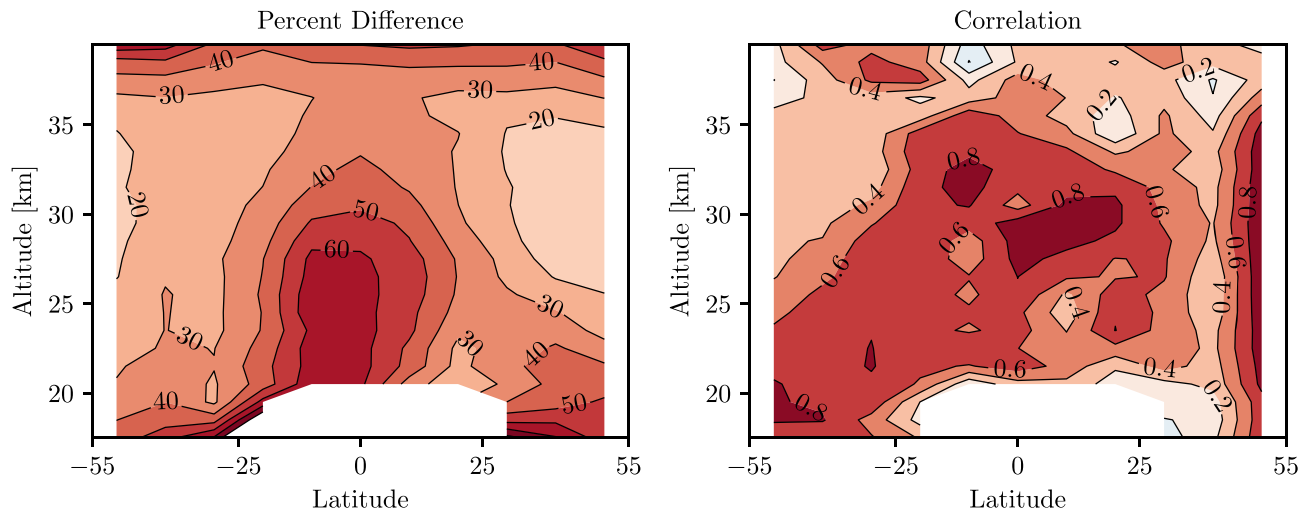


Figure 7. Left: Mean percent difference between SAGE II sunset and OSIRIS NO₂ at 12:00 p.m. during the overlap period. Right: Mean correlation between SAGE II sunset and OSIRIS NO₂ at 12:00 p.m. during the overlap period.

the anomaly time series given the reasonable correlation between the data sets throughout much of the stratosphere. The decreased correlation above 25 km south of 30° S and at all altitudes near 40° N indicate regions that must be analyzed with caution. Note that in these regions the lower correlation is likely due to the increased noise and reduced variability in the data.

PRATMO can also be used to convert the measured NO₂ to NO_x in order to compare directly with NO_x from WACCM. The photochemical model outputs NO and NO₂ which can be added together to get the model NO_x. Then the estimated measured NO_x can be found by using the ratio

$$[\text{NO}_x]^{meas.} = [\text{NO}_2]^{meas.} \frac{[\text{NO}_x]^{model}}{[\text{NO}_2]^{model}}. \quad (5)$$

The NO_x is calculated for each measurement after it has been shifted to 12:00 p.m. Note that PRATMO and WACCM have consistent NO_x diurnal cycles. This was tested using a subset of hourly sampled WACCM output.

4. Merging

The SAGE II sunset and OSIRIS NO₂ are merged following the process used to merge SAGE II and OSIRIS ozone in Bourassa et al. (2014). The first step is to determine the mean bias between the two instruments for each latitude and altitude bin. This is done by first grouping the data by month and finding the average difference between the instruments for each month when both instruments have data and then taking the average of these monthly values. The mean bias is subtracted from the SAGE II NO₂ so that it is on the same scale as OSIRIS. Figure 8 shows the monthly zonal mean SAGE II sunset and OSIRIS NO₂ in four altitude and latitude bins after the bias is removed from the SAGE II data.

Each data set is then deseasonalized individually by subtracting the means of each month to account for differences in the instrument sampling. Finally, the deseasonalized SAGE II sunset and OSIRIS NO₂ monthly means are combined into a single time series by taking the unweighted average value in months when both instruments have data. The same merging process is repeated with the NO_x from SAGE II and OSIRIS that was calculated with PRATMO. This merged NO_x is used in the remainder of the analysis so that the results can be compared with NO_x from WACCM.

The deseasonalized relative anomalies of the merged SAGE II-OSIRIS NO_x are given in Figure 9 for four altitude and latitude bins. The corresponding WACCM NO_x deseasonalized relative anomalies are also shown in Figure 9. The WACCM NO_x was sampled as daily averages, which were then used to compute the monthly means. Although this results in different absolute values than we have for the observational data

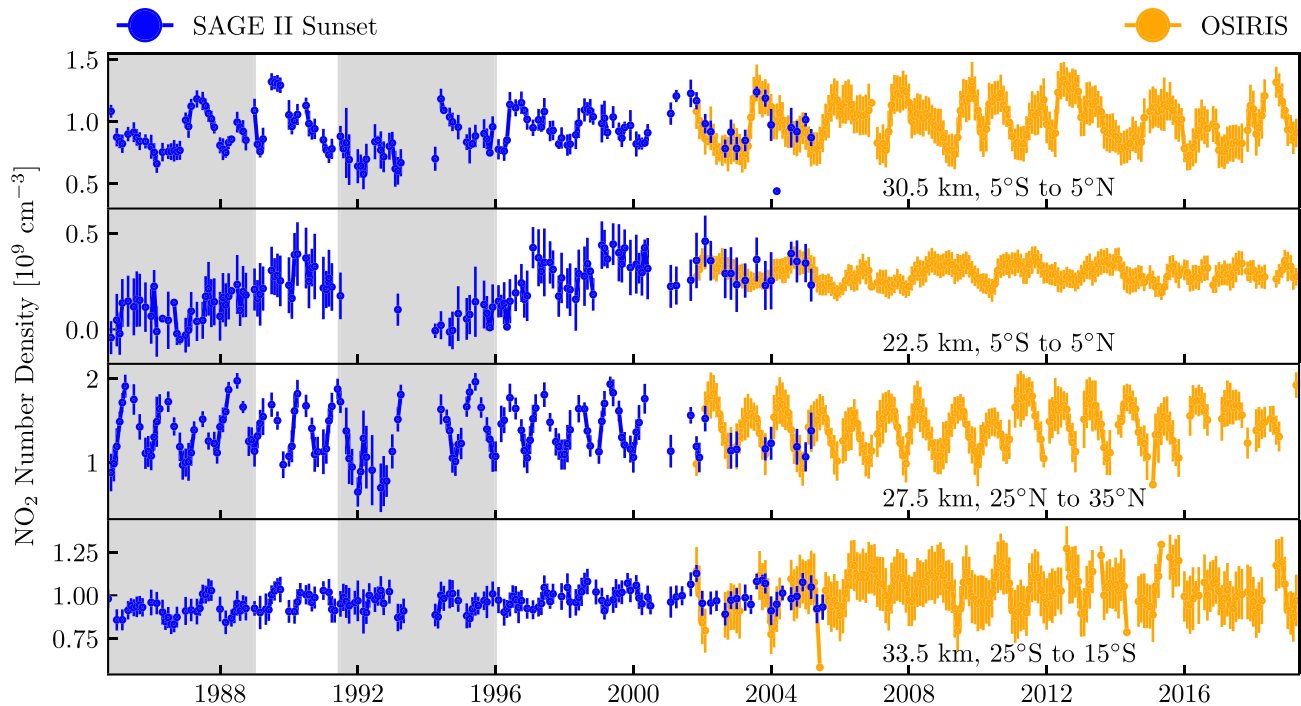


Figure 8. Monthly zonal mean SAGE II sunset and OSIRIS NO_2 at 12:00 p.m. after the bias has been subtracted from SAGE. The shaded regions denote the time periods influenced by large volcanic eruptions.

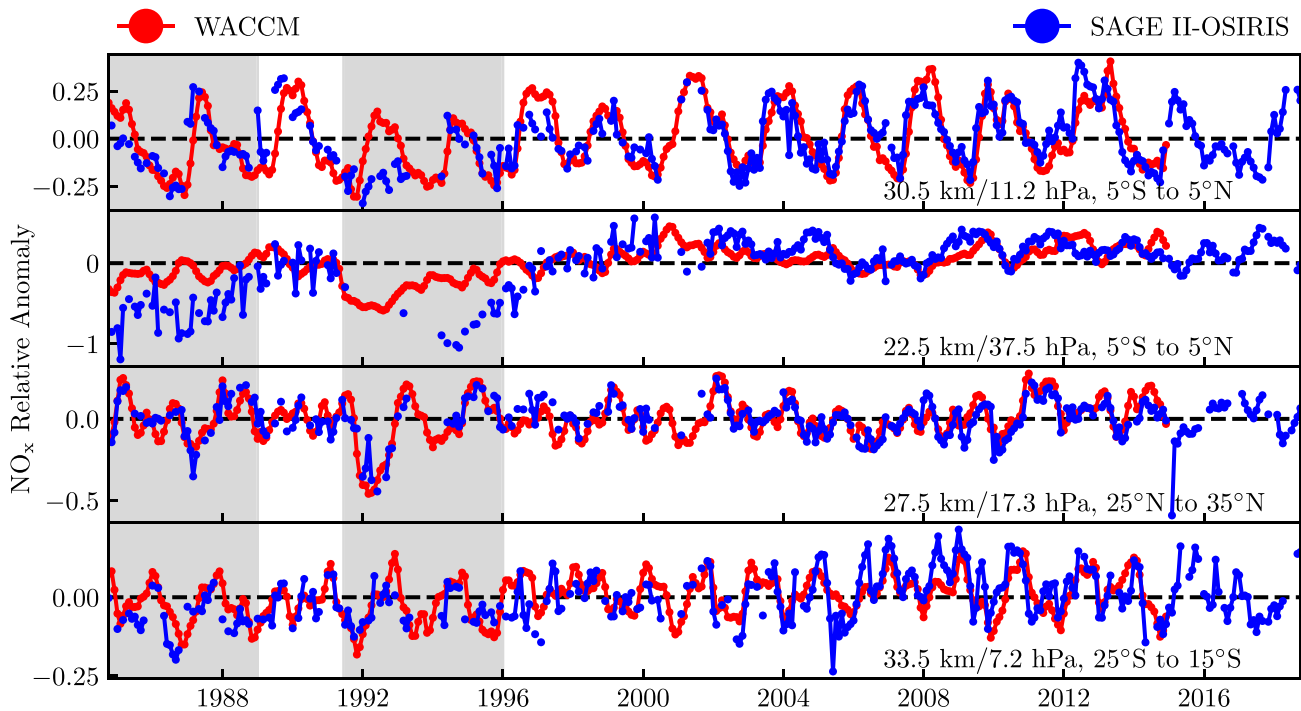


Figure 9. Relative anomaly of merged SAGE II sunset and OSIRIS NO_x at 12:00 p.m. in four latitude and altitude bins, as well as the relative anomaly of WACCM NO_x . The shaded regions denote the time periods influenced by large volcanic eruptions.

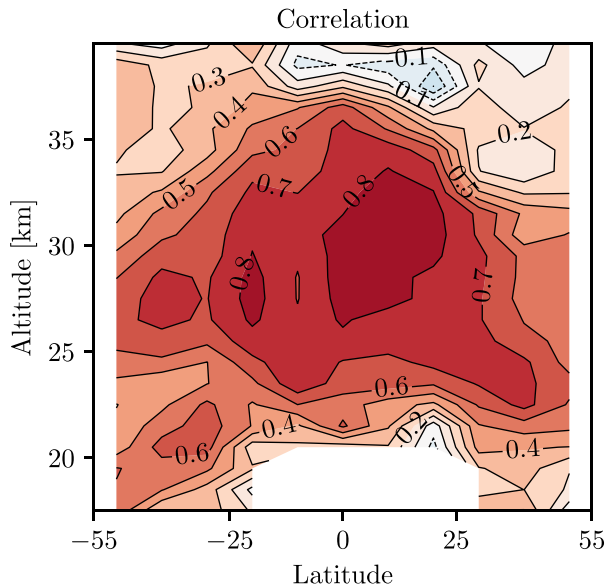


Figure 10. Correlation coefficient for merged SAGE II sunset and OSIRIS NO_x correlated with WACCM NO_x .

at 12:00 p.m., the fractional changes are the same, so we can compare the relative anomalies from the model and observations.

The top panel of Figure 9 shows that the QBO is clear in both data sets near 30 km in the tropics, with consistent phase and amplitude between the model and observations. This is consistent with previous results from Park et al. (2017). Both WACCM and SAGE II-OSIRIS also show similar variations outside of the tropics, as can be seen in the bottom two panels of Figure 9. The observations and WACCM results differ near 22 km in the tropics, where the observations show a larger negative anomaly than WACCM during periods associated with the El Chichon, Nevado del Ruiz, and Pinatubo volcanic eruptions.

Figure 10 shows the correlation between the merged SAGE II-OSIRIS NO_x and the WACCM NO_x , excluding the volcanic periods. In order to calculate the correlation coefficient, the WACCM data had to be interpolated to an altitude grid so the values are approximate. The correlation is greater than 0.7 in much of the stratosphere, with lower values at the highest and lowest altitudes.

5. Linear Regression

Variability and linear trends in the merged and deseasonalized monthly zonal mean data set are determined using a linear regression model. This type of model has often been used to quantify trends and variations in stratospheric ozone (e.g., Bourassa et al., 2018; Harris et al., 2015; Kuttippurath & Nair, 2017; Steinbrecht et al., 2017) and NO_2 (e.g., Galytska et al., 2019; Liley et al., 2000; Zawodny & McCormick, 1991).

Linear regression models that are used to study stratospheric composition typically include terms to represent the QBO, the El Niño-Southern Oscillation (ENSO), the 11-year solar cycle, and volcanic aerosol, as well as seasonal oscillations. For each latitude and altitude bin the linear regression equation is

$$[\text{NO}_x] = A^{(2)} + B \times \text{linear}(t) + C^{(2)} \times \text{QBO}_a(t) + D^{(2)} \times \text{QBO}_b(t) + E \times F_{10.7}(t) + F \times \text{ENSO}(t) + G \times \text{GloSSAC}(t) + R(t). \quad (6)$$

The capital letters A through G are the regression coefficients, and the superscripts specify the number of the highest seasonal harmonics included for a given term. This value corresponds to n in the seasonal harmonic equation,

$$1 + \sum_{i=1}^n \left(\sin\left(\frac{2\pi}{365.25}it\right) + \cos\left(\frac{2\pi}{365.25}it\right) \right). \quad (7)$$

In total there are 19 regression coefficients: seven corresponding to A through G in equation 6, plus four coefficients from the first and second harmonics of the constant, $\text{QBO}_a(t)$, and $\text{QBO}_b(t)$ terms.

In equation (6), $\text{QBO}_a(t)$ and $\text{QBO}_b(t)$ are the first two principal components of the Singapore zonal winds (Wallace et al., 1993), $F_{10.7}(t)$ is the solar flux at 10.7 cm, $\text{ENSO}(t)$ is the multivariate ENSO index, and $R(t)$ is the residual. The regression code and these predictors are described in detail in SPARC/IO3C/GAW (2019). The $\text{GloSSAC}(t)$ term is the monthly mean aerosol extinction anomaly, which is different for each latitude and altitude bin. GloSSAC is the Global Space-based Stratospheric Aerosol Climatology, derived from space-based measurements of aerosol from 1979 to 2016, including measurements from SAGE II and OSIRIS, as well as the Cloud-Aerosol Lidar with Orthogonal Polarization instrument (CALIOP), the Cryogenic Limb Array Etalon Spectrometer (CLAES), and others. The data set is described in Thomason et al. (2018).

It was found that using a form of the regression model without seasonal harmonics did not account for some of the variability in the data, despite the fact that the data had been deseasonalized. Most clearly, the regression did not capture the full QBO in the midstratosphere. The extratropical QBO circulation (and its effects on constituents) is modulated by the annual cycle, with the strongest effects in the winter hemisphere

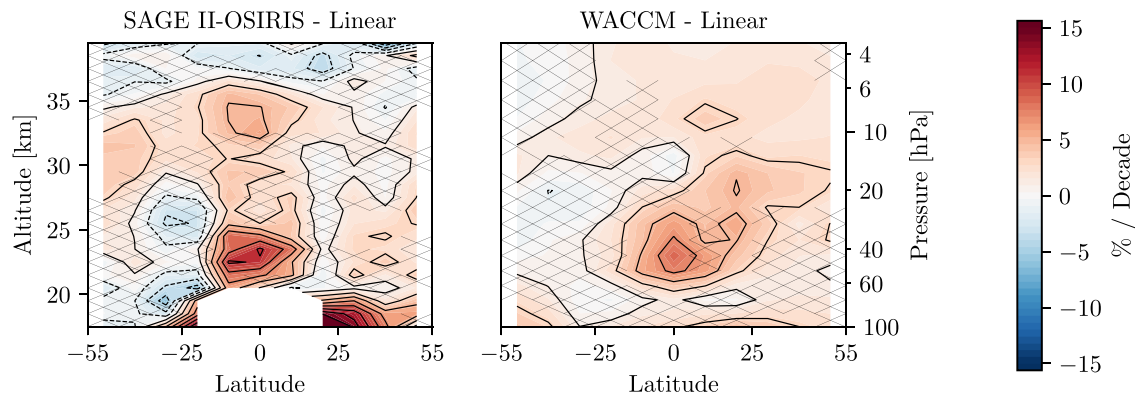


Figure 12. Linear trend in SAGE II-OSIRIS NO_x and WACCM NO_x . The contour intervals are 2% per decade.

blue) the large volcanoes for WACCM are also included in the figure. The right panel of Figure 11 shows the aerosol coefficients for the same scenarios. For the satellite observations the aerosol coefficients clearly become much more negative when the volcanic periods are included, and the trends are a factor of three larger. Such large trends are mainly the result of fitting the large negative NO_x anomalies associated with El Chichon at the beginning of the time series (see Figure 9). Including the volcanic time periods has a comparatively much smaller effect on WACCM. The trend is similar in both the cases with and without an aerosol predictor in the regression, even when there is a clear aerosol effect in the data. This is because the aerosol term is dominated by fitting Pinatubo (as discussed above) and has little influence on the negative anomalies tied to El Chichon. Because of this sensitivity, we conclude that the trends are more realistically estimated from the data by omitting the volcanic time periods. Including the volcanic time periods has a comparatively much smaller effect on WACCM.

Due to the better agreement between the observations and WACCM, the volcanic periods were omitted to find the latitudinal structure of the linear trends shown in Figure 12 so that the variability between the two data sets could be easily compared. The hatched regions in Figure 12 are statistically insignificant. The Figure shows that both SAGE II-OSIRIS and WACCM have a maximum trend near 22 km in the tropics: For the measurements the maximum trend is around $10\% \pm 3\%$ per decade, while for WACCM it is about $7\% \pm 5\%$ per decade. These trends are equivalent within the statistical uncertainties. The SAGE II-OSIRIS data show a secondary relative trend maximum from 32 to 35 km in the tropics of around $5\% \pm 3\%$ per decade, which is not seen in WACCM. In both cases the positive trend is only significant outside of the tropics from about 25 to 35 km. SAGE II-OSIRIS shows this significant, positive trend in both hemispheres, while for WACCM it is much more prominent in the Northern Hemisphere. Overall, we can say that WACCM accurately represents observed NO_x changes in the tropics.

Figure 13 compares the linear regression model to the SAGE II-OSIRIS NO_x relative anomaly in four bins. The model captures many of the large variations in the data. This can be quantified by examining the fraction of variance explained by the regression, which is calculated as the variance of the regression model divided by the variance of the data. The left panel of Figure 14 shows the fraction of the total variance in the SAGE II-OSIRIS data explained by the regression model, while the right panel shows the fraction of the variance in WACCM explained by the regression model. The volcanic periods are omitted when calculating the fraction as they were not fit by the regression. The regression accounts for much of the variability in the observations in the tropics above 20 km. The fraction is greatest in regions where the data shows the most variability from the QBO and linear trend.

Overall, the regression fits the data well, except during volcanic periods at lower altitudes (second panel of Figure 13). Although an aerosol term is included in the regression, it does not capture the prolonged decrease in NO_x that was measured by SAGE II. Note that the results of the regression look remarkably similar to the WACCM NO_x shown in Figure 9. This difference suggests either possible problems with the SAGE II data following large volcanic eruptions or poor understanding of the NO_x response to large volcanoes. Previous studies by Randel et al. (1999, 2000) compared sunset NO_2 from SAGE II to sunset NO_2 from HALOE from 1991 to 1998 and found that the HALOE NO_2 showed the same slow recovery from Pinatubo as the SAGE II NO_2 in the tropics. This similarity suggests that the SAGE II observations in the years following Pinatubo

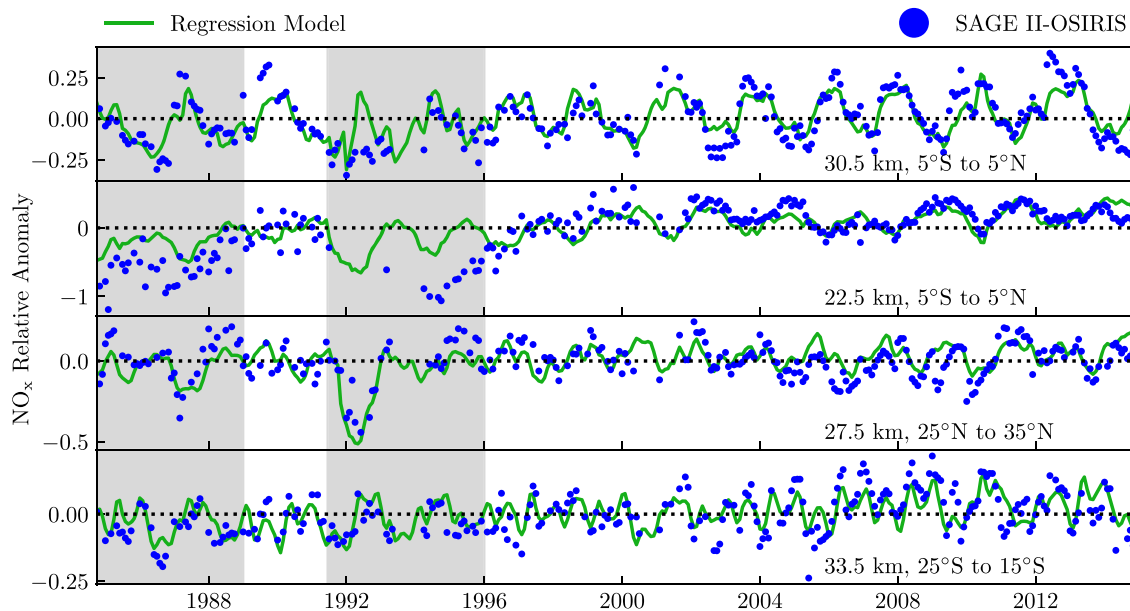


Figure 13. Monthly mean relative anomaly of merged SAGE II sunset and OSIRIS NO_x compared to the linear regression model, including an aerosol term, in four latitude and altitude bins.

are correct, despite the disagreement with WACCM and the inability of the aerosol term in the regression to capture the full variability. The variations in HALOE and SAGE II NO_2 were also shown to be consistent with an observed decrease in HNO_3 from MLS on UARS over the period from 1993 to 1997. The fact that WACCM NO_x recovers much more quickly from Pinatubo than NO_x from the satellite instruments shows that we do not yet have a good understanding of, and therefore ability to model, the effect of large amounts of volcanic aerosol on NO_x in the stratosphere.

Galytska et al. (2019) derived a 15% per decade increase in SCIAMACHY NO_2 in the tropics from 30 to 35 km over the years 2004 to 2012. In this same region the increase in the SAGE II-OSIRIS data set is only 5% per decade from 1984 to 2014. Galytska et al. (2019) also observed a significant decrease in NO_2 in the Southern Hemisphere and increase in the Northern Hemisphere extratropics which is visible, although insignificant, in the longer time series presented here (Figure 12). They associated a decline in O_3 with the increase in NO_2 . The linear trend in the SAGE II-OSIRIS data from only 2004 to 2012 is shown in Figure 15. This result is similar to the findings shown in Figure 2 of Galytska et al. (2019). There is a negative trend of up to -20% per decade in the Southern Hemisphere and a positive trend of up to 20% per decade in the Northern Hemisphere. There is a 15% to 20% per decade increase in NO_x in the tropics from 30 to 35 km.

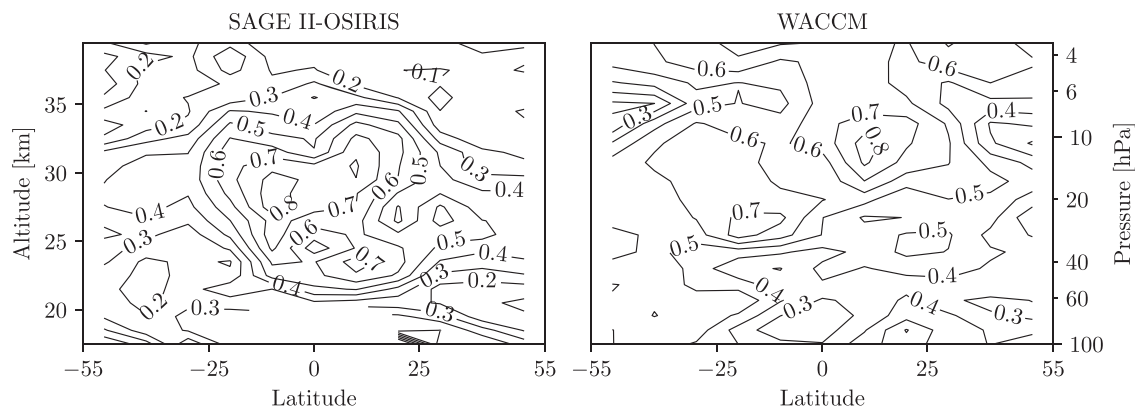


Figure 14. Fraction of variance explained by the linear regression model for SAGE II-OSIRIS NO_x and WACCM NO_x . This calculation omits the large volcanic time periods (shaded regions in Figure 13).

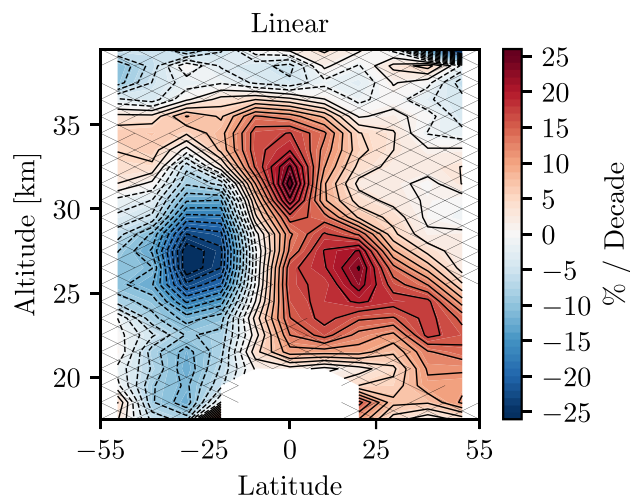


Figure 15. Linear trend in SAGE II-OSIRIS data from 2004 to 2012. The contour intervals are 2% per decade.

6. Conclusion

The SAGE II sunset NO_2 measurements have been merged with NO_2 measurements from OSIRIS to produce a data set of monthly zonal mean NO_2 spanning from 1984 to 2018. The merging required the use of the PRATMO photochemical box model to shift the SAGE II and OSIRIS measurements to a common local solar time in order to account for the diurnal cycle in NO_2 . Both data sets were shifted to 12:00 p.m. local time, where the NO_2 concentration is relatively stable. The resulting data sets retain a near-constant, although smaller, bias between SAGE II and OSIRIS, but correlations of at least 0.6 at most latitudes from 25 to 34 km during the overlap period (Figure 7). This common variability enhances confidence in creating a merged NO_2 data set from occultation and limb-scattering measurements. The photochemical model was also used to convert the measured NO_2 into NO_x for comparison with NO_x from WACCM. The merged SAGE II-OSIRIS NO_x relative anomalies show good correlation with WACCM over most of the globe, away from the periods following large volcanic eruptions (Figures 9 and 10). This agreement further enhances confidence in the merged and photochemically corrected SAGE II-OSIRIS NO_x data set.

We applied a standard linear regression model to the merged data in order to quantify NO_x variability tied to the QBO, linear trends, and volcanic aerosol. The QBO coefficients (not shown) have similar structure and values to those derived by Park et al. (2017) using OSIRIS and WACCM NO_x from 2005 to 2014, with good agreement between observational and model results. The novel information here regards the long-term trends and volcanic aerosol fits in the regressions. We find that the statistical regression fits for these terms are very different whether or not the periods following the large volcanic eruptions of El Chichon 1982 and Pinatubo 1991 are included in the regression fits. Including these periods results in unphysically large trends and aerosol regression coefficients (Figure 11), and we therefore focus on results omitting these periods (i.e., regression fits are calculated based on data for 1989 to May 1991 and 1996 to 2014).

The derived linear trends from the merged SAGE II-OSIRIS data over the years 1984 to 2014 show NO_x increases of 8–10% per decade centered in the tropical lower stratosphere (around 22 to 25 km). The trends in the WACCM model have similar spatial structure, with slightly smaller maximum values of about 6–7% per decade. Given the statistical uncertainties from the relatively short data record ($\sim \pm 4\%$ per decade), this represents reasonable agreement between observed and modelled long-term trends. The observations show a secondary tropical NO_x trend maximum of around 5% per decade from 32 to 35 km that is marginally significant, and which is not found in WACCM. The observed trends, which are greater than the trend of around 2.4% per decade in N_2O , also agree with previous findings that stratospheric NO_x trends are only partially due to increasing tropospheric N_2O .

As a note, trend analysis of the merged SAGE II-OSIRIS data based only on the years 2004 to 2012 produces large trend values similar to those derived Galytska et al. (2019) using SCIAMACHY NO_2 measurements (Figure 15). The good agreement in the results for the same analysis period promotes further confidence in the merged SAGE II-OSIRIS data record. However, these large trends mainly represent variability over

a relatively short 8-year data record and are not representative of the longer term trends derived from the merged SAGE II-OSIRIS data record.

Acknowledgments

The OSIRIS project is funded in part by the Canadian Space Agency, and the Odin satellite project is funded by the Swedish National Space Agency, and by the European Space Agency as a Third Party Mission. We thank the SAGE II Team at NASA Langley for ongoing support of the SAGE II data and collaboration. OSIRIS NO₂ data and the merged SAGE II-OSIRIS NO_x are publicly available under the headings Level 2 and Level 3, respectively, at <https://research-groups.usask.ca/osiris/data-products.php>. SAGE II data are publicly available at <https://eosweb.larc.nasa.gov/project/sage2/sage2&urlscore=v7&urlscore;table>. The regression code and predictor data is available at <https://arg.usask.ca/docs/LOTUS&urlscore;regression/index.html>. Thanks to Chris Roth for aid in running the PRATMO model.

References

Adams, C., Bourassa, A. E., McLinden, C. A., Sioris, C. E., von Clarmann, T., Funke, B., et al. (2017). Effect of volcanic aerosol on stratospheric NO₂ and N₂O₅ from 2002–2014 as measured by Odin-OSIRIS and Envisat-MIPAS. *Atmospheric Chemistry and Physics*, 17(13), 8063–8080. <https://doi.org/10.5194/acp-17-8063-2017>

Barath, F. T., Chavez, M. C., Cofield, R. E., Flower, D. A., Frerking, M. A., Gram, M. B., et al. (1993). The upper atmosphere research satellite microwave limb sounder instrument. *Journal of Geophysical Research*, 98(D6), 10,751–10,762. <https://doi.org/10.1029/93JD00798>

Bodeker, G. E., Boyd, I. S., & Matthews, W. A. (1998). Trends and variability in vertical ozone and temperature profiles measured by ozonesondes at Lauder, New Zealand: 1986–1996. *Journal of Geophysical Research*, 103(D22), 28,661–28,681. <https://doi.org/10.1029/98JD02581>

Bourassa, A. E., Degenstein, D. A., Randel, W. J., Zawodny, J. M., Kyrölä, E., McLinden, C. A., et al. (2014). Trends in stratospheric ozone derived from merged SAGE II and Odin-OSIRIS satellite observations. *Atmospheric Chemistry and Physics*, 14(13), 6983–6994. <https://doi.org/10.5194/acp-14-6983-2014>

Bourassa, A. E., McLinden, C. A., Sioris, C. E., Brohede, S., Bathgate, A. F., Llewellyn, E. J., & Degenstein, D. A. (2011). Fast NO₂ retrievals from Odin-OSIRIS limb scatter measurements. *Atmospheric Measurement Techniques*, 4(5), 965–972. <https://doi.org/10.5194/amt-4-965-2011>

Bourassa, A. E., Roth, C. Z., Zawada, D. J., Rieger, L. A., McLinden, C. A., & Degenstein, D. A. (2018). Drift-corrected odin-OSIRIS ozone product: Algorithm and updated stratospheric ozone trends. *Atmospheric Measurement Techniques*, 11(1), 489–498. <https://doi.org/10.5194/amt-11-489-2018>

Brasseur, G. P., & Solomon, S. (2005). *Aeronomy of the middle atmosphere* (3rd ed., Vol. 32). Dordrecht, The Netherlands: Springer.

Damadeo, R. P., Zawodny, J. M., Thomason, L. W., & Iyer, N. (2013). SAGE version 7.0 algorithm: Application to SAGE II. *Atmospheric Measurement Techniques*, 6(12), 3539–3561. <https://doi.org/10.5194/amt-6-3539-2013>

Galytska, E., Rozanov, A., Chipperfield, M. P., Dhomse, S. S., Weber, M., Arosio, C., et al. (2019). Dynamically controlled ozone decline in the tropical mid-stratosphere observed by SCIAMACHY. *Atmospheric Chemistry and Physics*, 19(2), 767–783. <https://doi.org/10.5194/acp-19-767-2019>

Gray, L. J., & Dunkerton, T. J. (1990). The role of the seasonal cycle in the quasi-biennial oscillation of ozone. *Journal of the Atmospheric Sciences*, 47(20), 2429–2452. [https://doi.org/10.1175/1520-0469\(1990\)047<2429:TROTSC>2.0.CO;2](https://doi.org/10.1175/1520-0469(1990)047<2429:TROTSC>2.0.CO;2)

Haley, C. S., Brohede, S. M., Sioris, C. E., Griffioen, E., Murtagh, D. P., McDade, I. C., et al. (2004). Retrieval of stratospheric O₃ and NO₂ profiles from Odin optical spectrograph and infrared imager system (OSIRIS) limb-scattered sunlight measurements. *Journal of Geophysical Research*, 109, D16303. <https://doi.org/10.1029/2004JD004588>

Harris, N. R. P., Hassler, B., Tummon, F., Bodeker, G. E., Hubert, D., Petropavlovskikh, I., et al. (2015). Past changes in the vertical distribution of ozone Part 3: Analysis and interpretation of trends. *Atmospheric Chemistry and Physics*, 15(17), 9965–9982. <https://doi.org/10.5194/acp-15-9965-2015>

Hartmann, D. L., Klein Tank, A. M. G., Rusticucci, M., Alexander, L. V., Brönnimann, S., Charabi, Y., et al. (2013). Observations: Atmosphere and surface. In T. F. Stocker, D. Qin, G.-K. Plattner, M. Tignor, S. K. Allen, et al. (Eds.), *Climate change 2013: The physical science basis. Contribution of working group I to the fifth assessment report of the intergovernmental panel on climate change* (pp. 159–254). Cambridge, United Kingdom and New York, NY, USA: Cambridge University Press. <https://doi.org/10.1017/CBO9781107415324.008>

Kuttippurath, J., & Nair, P. J. (2017). The signs of Antarctic ozone hole recovery. *Scientific Reports*, 7(1), 585.

Liley, J. B., Johnston, P. V., McKenzie, R. L., Thomas, A. J., & Boyd, I. S. (2000). Stratospheric NO₂ variations from a long time series at Lauder, New Zealand. *Journal of Geophysical Research*, 105(D9), 11,633–11,640. <https://doi.org/10.1029/1999JD901157>

Llewellyn, E. J., Lloyd, N. D., Degenstein, D. A., Gattinger, R. L., Petelina, S. V., Bourassa, A. E., et al. (2004). The OSIRIS instrument on the Odin spacecraft. *Canadian Journal of Physics*, 82(6), 411–422. <https://doi.org/10.1139/p04-005>

Marsh, D. R., Mills, M. J., Kinnison, D. E., Lamarque, J.-F., Calvo, N., & Polvani, L. M. (2013). Climate change from 1850 to 2005 simulated in CESM1(WACCM). *Journal of Climate*, 26(19), 7372–7391. <https://doi.org/10.1175/JCLI-D-12-00558.1>

McLinden, C. A., Olsen, S. C., Hannegan, B., Wild, O., Prather, M. J., & Sundet, J. (2000). Stratospheric ozone in 3-D models: A simple chemistry and the cross-tropopause flux. *Journal of Geophysical Research*, 105(D11), 14,653–14,665. <https://doi.org/10.1029/2000JD900124>

McLinden, C. A., Olsen, S. C., Prather, M. J., & Liley, J. B. (2001). Understanding trends in stratospheric NO_y and NO₂. *Journal of Geophysical Research*, 106(D21), 27,787–27,793. <https://doi.org/10.1029/2000JD000100>

Morgenstern, O., Hegglin, M. I., Rozanov, E., O'Connor, F. M., Abraham, N. L., Akiyoshi, H., et al. (2017). Review of the global models used within phase 1 of the Chemistry–Climate Model Initiative (CCMI). *Geoscientific Model Development*, 10(2), 639–671. <https://doi.org/10.5194/gmd-10-639-2017>

Murtagh, D., Frisk, U., Merino, F., Ridal, M., Jonsson, A., Stegman, J., et al. (2002). An overview of the odin atmospheric mission. *Canadian Journal of Physics*, 80(4), 309–319. <https://doi.org/10.1139/p01-157>

Park, M., Randel, W. J., Kinnison, D. E., Bourassa, A. E., Degenstein, D. A., Roth, C. Z., et al. (2017). Variability of stratospheric reactive nitrogen and ozone related to the QBO. *Journal of Geophysical Research: Atmospheres*, 122, 10,103–10,118. <https://doi.org/10.1002/2017JD027061>

Prather, M. J. (1992). Catastrophic loss of stratospheric ozone in dense volcanic clouds. *Journal of Geophysical Research*, 97(D9), 10,187–10,191. <https://doi.org/10.1029/92JD00845>

Prather, M. J., Hsu, J., DeLuca, N. M., Jackman, C. H., Oman, L. D., Douglass, A. R., et al. (2015). Measuring and modeling the lifetime of nitrous oxide including its variability. *Journal of Geophysical Research: Atmospheres*, 120, 5693–5705. <https://doi.org/10.1002/2015JD023267>

Randel, W. J., Polvani, L., Wu, F., Kinnison, D. E., Zou, C.-Z., & Mears, C. (2017). Troposphere-stratosphere temperature trends derived from satellite data compared with ensemble simulations from WACCM. *Journal of Geophysical Research: Atmospheres*, 122, 9651–9667. <https://doi.org/10.1002/2017JD027158>

Randel, W. J., Wu, F., Russell III, J. M., & Waters, J. (1999). Space-time patterns of trends in stratospheric constituents derived from UARS measurements. *Journal of Geophysical Research*, 104(D3), 3711–3727. <https://doi.org/10.1029/1998JD100044>

- Randel, W. J., Wu, F., Russell III, J. M., Zawodny, J. M., & Nash, J. (2000). Interannual changes in stratospheric constituents and global circulation derived from satellite data. In Siskind, D. E., Eckermann, S. D., & Summers, M. E. (Eds.), *Geophysical monograph series: Atmospheric science across the stratopause* (Vol. 123). Washington DC: American Geophysical Union, pp. 271–285.
- Randel, W. J., Wu, F., Swinbank, R., Nash, J., & O'Neill, A. (1999). Global QBO circulation derived from UKMO stratospheric analyses. *Journal of the Atmospheric Sciences*, *56*(4), 457–474. [https://doi.org/10.1175/1520-0469\(1999\)056<0457:GQCDFU>2.0.CO;2](https://doi.org/10.1175/1520-0469(1999)056<0457:GQCDFU>2.0.CO;2)
- Ravishankara, A. R., Daniel, J. S., & Portmann, R. W. (2009). Nitrous Oxide (N₂O): The dominant ozone-depleting substance emitted in the 21st century. *Science*, *326*(5949), 123–125. <https://doi.org/10.1126/science.1176985>
- Rieger, L. A., Bourassa, A. E., & Degenstein, D. A. (2015). Merging the OSIRIS and SAGE II stratospheric aerosol records. *Journal of Geophysical Research: Atmospheres*, *120*, 8890–8904. <https://doi.org/10.1002/2015JD023133>
- Russell, III, Gordley, L. L., Park, J. H., Drayson, S. R., Hesketh, W. D., Cicerone, R. J., et al. (1993). The halogen occultation experiment. *Journal of Geophysical Research*, *98*(D6), 10,777–10,797. <https://doi.org/10.1029/93JD00799>
- SPARC/IO3C/GAW (2019). SPARC/IO3C/GAW report on long-term ozone trends and uncertainties in the stratosphere. In Petropavlovskikh, I., Godin-Beekmann, S., Hubert, D., Damadeo, R., Hassler, B., & Sofieva, V. (Eds.), *SPARC report N° 9 (2019) of The SPARC LOTUS activity* (Chap. 4, pp. 37–50). Oberpfaffenhofen: SPARC Report No. 9, GAW Report No. 241, WCRP-17/2018. <https://doi.org/10.17874/f899e57a20b>
- Seinfeld, J. H., & Pandis, S. N. (2006). *Atmospheric chemistry and physics: From air pollution to climate change* (2nd ed.). Hoboken, New Jersey: John Wiley.
- Sioris, C. E., Rieger, L. A., Lloyd, N. D., Bourassa, A. E., Roth, C. Z., Degenstein, D. A., et al. (2017). Improved OSIRIS NO₂ retrieval algorithm: Description and validation. *Atmospheric Measurement Techniques*, *10*(3), 1155–1168. <https://doi.org/10.5194/amt-10-1155-2017>
- Steinbrecht, W., Froidevaux, L., Fuller, R., Wang, R., Anderson, J., Roth, C., et al. (2017). An update on ozone profile trends for the period 2000 to 2016. *Atmospheric Chemistry and Physics*, *17*(17), 10,675–10,690. <https://doi.org/10.5194/acp-17-10675-2017>
- Thomason, L. W., Ernest, N., Millán, L., Rieger, L., Bourassa, A., Vernier, J.-P., et al. (2018). A global space-based stratospheric aerosol climatology: 1979–2016. *Earth System Science Data*, *10*(1), 469–492. <https://doi.org/10.5194/essd-10-469-2018>
- Wallace, J. M., Panetta, R. L., & Estberg, J. (1993). Representation of the equatorial stratospheric quasi-biennial oscillation in EOF phase space. *Journal of the Atmospheric Sciences*, *50*(12), 1751–1762. [https://doi.org/10.1175/1520-0469\(1993\)050h1751:ROTESQi2.0.CO;2](https://doi.org/10.1175/1520-0469(1993)050h1751:ROTESQi2.0.CO;2)
- Waters, J. W., Froidevaux, L., Harwood, R. S., Jarnot, R. F., Pickett, H. M., Read, W. G., et al. (2006). The Earth observing system microwave limb sounder (EOS MLS) on the Aura Satellite. *IEEE Transactions on Geoscience and Remote Sensing*, *44*(5), 1075–1092. <https://doi.org/10.1109/TGRS.2006.873771>
- Zawodny, J. M., & McCormick, M. P. (1991). Stratospheric Aerosol and Gas Experiment II measurements of the quasi-biennial oscillations in ozone and nitrogen dioxide. *Journal of Geophysical Research*, *96*, 9371–9377. <https://doi.org/10.1029/91JD00517>
- Bovensmann, H., Burrows, J. P., Buchwitz, M., Frerick, J., Nol, S., Rozanov, V. V., et al. SCIAMACHY: Mission objectives and measurement modes. *Journal of the Atmospheric Sciences*, *56*(2), 127–150. [https://doi.org/10.1175/1520-0469\(1999\)056h0127:SMOAMMi2.0.CO;2](https://doi.org/10.1175/1520-0469(1999)056h0127:SMOAMMi2.0.CO;2)